Engineering Chemistry
ISSN: 2813-6535, Vol. 13, pp 7-14
doi:10.4028/p-RvQ1bZ

Submitted: 2024-11-29
Accepted: 2025-10-10
Online: 2026-02-18

Microkinetic Comparison of CO_2 Hydrogenation to Methanol over Unsupported and Supported Subnanometer Pd_x Clusters

Dzaki Ahmad Syaifullah[1,a], Muhammad Arkan Nuruzzahran[1,b], Abel Pradipta Wijaya[1,c], Azhar Ikhtiarudin[1,d], Reva Budiantono[1,e], Muhammad Haris Mahyuddin[1,2,f] and Adhitya Gandaryus Saputro[1,2,g *]

[1]Quantum and Nano Technology Research Group, Faculty of Industrial Technology, Institut Teknologi Bandung, Bandung, West Java 40132, Indonesia

[2]Research Centre for Nanoscience and Nanotechnology, Institut Teknologi Bandung, Bandung, West Java 40132, Indonesia

[a]dzakiahmad2002@gmail.com, [b]arkannuruzzahran@gmail.com, [c]abelpw.x@gmail.com, [d]azharikhtiarudin@gmail.com, [e]budiantonoreva@gmail.com, [f]mahyuddin133@itb.ac.id, [g]gandaryus@itb.ac.id

Keywords: methanol, CO_2 hydrogenation, microkinetic, subnanometer Pd cluster, transition metal oxides

Abstract. A promising approach to meet rising energy demands while mitigating environmental risks from greenhouse gases is the conversion of carbon dioxide into methanol through CO_2 hydrogenation. Previous studies have demonstrated that unsupported subnanometer Pd_x clusters exhibit excellent performance in this conversion. However, the influence of support materials on the activity of Pd clusters remains poorly understood. In this study, we compare the kinetics of CO_2 hydrogenation to methanol using unsupported Pd_7 clusters and those supported by metal oxides, specifically $Pd_4/In_2O_3(110)$ and $Pd_3/TiO_2(110)$. Microkinetic simulations, based on available energetic data from the literatures, reveal that $Pd_4/In_2O_3(110)$ delivers superior kinetic performance, followed by Pd_7 and $Pd_3/TiO_2(110)$. These findings demonstrate that the choice of support material plays a critical role in dictating the reaction pathway and rate for supported Pd cluster catalysts.

Introduction

The increasing concentration of carbon dioxide (CO_2) in the atmosphare is one of the main causes of global warming and climate change [1–3]. The conversion of CO_2 into methanol (CH_3OH) through a hydrogenation process ($CO_2 + 3H_2 \rightarrow H_2O + CH_3OH$), using hydrogen produced by electrolysis of water, is an alternative solution to reduce excess CO_2 emissions while producing valuable chemicals [4–6]. Methanol can be used as a liquid fuel in direct methanol fuel cells and as liquid hydrogen storage to reduce our dependence on fossil fuel [7,8]. The CO_2 hydrogenation process to produce methanol is conventionally carried out using $Cu/ZnO/Al_2O_3$ catalyst at high temperature and high pressure [1,9,10]. These operating conditions are necessary because CO_2 is a stable and inert molecule that interacts weakly with catalysts at ambient conditions [11–13]. This certainly makes the process of converting CO_2 to methanol economically expensive. For this reason, it is important to find catalysts which can operate at lower temperature and pressure.

Recent reports suggest that small size Pd cluster catalyst exhibit higher activity for CO_2 hydrogenation to methanol compared to conventional $Cu/ZnO/Al_2O_3$ catalyst [14]. The high activity is due to the good ability of Pd to adsorb and dissociate H_2 to provide hydrogen atoms required in the hydrogenation process of CO_2 [15]. Previous research by Saputro et al. has shown that subnanometer Pd_7 cluster exhibit good performance in the conversion of CO_2 to methanol [4,5]. The catalytic activity of Pd catalysts has also been reported to be enhanced by the addition of metal oxide support [15]. Metal oxide plays a role in stabilizing Pd clusters as it is able to interact strongly with Pd. In addition, metal oxide has a higher affinity toward CO_2, so it plays an important role in CO_2 adsorption [16]. Pd clusters that play a role in H_2 dissociation and metal oxide support on which CO_2 is adsorbed provide a synergistic effect, so that CO_2 hydrogenation can occur either on the metal oxide or at the

Pd-metal oxide interface [14,16]. Therefore, supported Pd clusters have a good potential to be used as catalysts for CO_2 hydrogenation.

Previous work by Ye et al. demonstrate that Pd_4 cluster supported on $In_2O_3(110)$ is a promising catalyst for methanol synthesis from CO_2 [16]. Another study by Ou et al. investigated the reaction mechanism of CO_2 hydrogenation to CH_3OH on $Pd_3/TiO_2(110)$ catalyst and found that the interface between Pd and support has a significant influence on the catalytic activity [14]. However, the mechanism study was only carried out thermodynamically by comparing the activation barrier and reaction energy between pathways to find the minimum energy reaction path. The kinetic performance of the catalyst has not been further investigated. Kinetic studies are necessary to gain knowledge about reaction rate and the effect of operating variables such as temperature on the reaction rate which can be used as a guide in conducting experiments. Herein, we compare the kinetics of CO_2 hydrogenation to methanol using unsupported Pd_7 cluster and those supported by metal oxides, specifically $In_2O_3(110)$ and $TiO_2(110)$. We perform microkinetic simulations based on energetic data from previous studies to observe the effect of metal oxide support on the reaction rate and the dominant reaction pathway in CO_2 hydrogenation process.

Methods

To investigate the kinetics of CO_2 hydrogenation to methanol, we performed detailed microkinetic simulations based on energies obtained from previous studies. The microkinetic model employed in this study follows a mean-field approach grounded in transition state theory (TST) [17]. Using this framework, we were able to simulate the reaction pathways and rates by numerically solving a set of ordinary differential equations (ODEs) that govern the coverage of a single surface species over time.

For the adsorption and desorption of species, we used the Hertz-Knudsen model, which provides rate expressions for these elementary steps. The adsorption rate constant k_{ads} was calculated as follows:

$$k_{\mathrm{ads}} = \frac{PA}{\sqrt{2\pi m k_{\mathrm{B}} T}} \exp\left(-\frac{E_{\mathrm{ads}}}{k_{\mathrm{B}} T}\right), \tag{1}$$

where P is the partial pressure of the molecule in the gas phase, A is the surface area available for adsorption, m is the molecular mass of the species (in kg), k_B is the Boltzmann constant, T is the temperature (in K), and E_{ads} is the adsorption energy. For desorption, the rate constant k_{des} was modeled as:

$$k_{\mathrm{des}} = 10^{13} \exp\left(-\frac{E_{\mathrm{des}}}{k_{\mathrm{B}} T}\right), \tag{2}$$

where E_{des} refers to the desorption energy in eV, which is crucial in determining how strongly the molecule interacts with the catalytic surface.

For surface reactions, the rate constants were expressed using the Arrhenius equation:

$$k = \frac{k_{\mathrm{B}} T}{h} \exp\left(-\frac{E_{\mathrm{act}}}{k_{\mathrm{B}} T}\right), \tag{3}$$

where E_{act} represents the activation barrier of the reaction in eV. Surface entropy changes were deemed negligible, and hence we omitted partition function ratios in these calculations. The microkinetic model captures the evolution of each species involved in the reaction by solving the following rate equation for fractional surface coverage θ_j:

$$\frac{d\theta_j}{dt} = \Sigma_k n_k r_k \tag{4}$$

where θ_j represents the fractional coverage of species j, n_k denotes the stoichiometric coefficient of the adsorbate in reaction step k, and r_k is the rate of reaction for that step.

This study presents a microkinetic model for the hydrogenation of CO_2 within the unsupported Pd_7, $Pd_3/TiO_2(110)$, and $Pd_4/In_2O_3(110)$ catalysts, focusing on formate and reverse water gas shift followed by CO hydrogenation (RWGS+CO) pathways. In the formate pathway, CO_2 reacts with hydrogen (H) to form intermediate formate (HCOO). The HCOO undergoes further hydrogenation to yield H_2COOH, which subsequently transforms into intermediate H_2CO and OH. The H_2CO can then proceed to generate methanol (CH_3OH), while the OH is converted into water (H_2O). This mechanism differs significantly from the RWGS+CO hydrogenation pathway. In the RWGS pathway, the process begins with the formation of intermediates such as HOCO or COOH, which then dissociate early into CO and OH. The CO undergoes hydrogenation to produce CH_3OH and the OH again being converted into H_2O.

Each catalyst exhibits distinct hydrogenation processes. As indicated by the data in Table 1, the formate pathway for the Pd_7 catalyst involves the following elementary reactions: RA0 → RA1 → RA2a → RA3a → RA4a → RA5a → RA6 → RA7 → RA8 → RA9 → RA10. Meanwhile, the RWGS+CO hydrogenation pathway for Pd_7 catalyst follows these elementary reactions: RA0 → RA1 → RA2b → RA3b → RA4b → RA6 → RA5b → RA7 → RA8 → RA9 → RA10. The table below summarizes the reaction pathways, activation barriers, reaction energies, and reaction rate equations of each elementary step for the unsupported Pd_7 catalyst [4].

Table 1. CO_2 hydrogenation step, energies, and reaction rates equation for Pd_7 [4].

Reaction Number	Reaction Notation	E_{act} [eV]	ΔE [eV]	Reaction Rates
RA0	$H_2 + 2* \rightarrow 2H*$	0	-0.73	$r_{A0} = k_{A0}P_{H_2}\theta_*^2 - k_{-A0}\theta_H^2$
RA1	$CO_2 + * \rightarrow CO_2*$	0	-0.21	$r_{A1} = k_{A1}P_{CO_2}\theta_* - k_{-A1}\theta_{CO_2}$
RA2a	$CO_2* + H* \rightarrow HCOO* + *$	0.93	-0.21	$r_{A2a} = k_{A2a}\theta_{CO_2}\theta_H - k_{-A2a}\theta_{HCOO}\theta_*$
RA2b	$CO_2* + H* \rightarrow HOCO* + *$	1.90	0.39	$r_{A2b} = k_{A2b}\theta_{CO_2}\theta_H - k_{-A2b}\theta_{HOCO}\theta_*$
RA3a	$HCOO* + H* \rightarrow HCOOH* + *$	1.16	0.94	$r_{A3a} = k_{A3a}\theta_{HCOO}\theta_H - k_{-A3a}\theta_{HCOOH}\theta_*$
RA3b	$HOCO* + H* \rightarrow CO* + OH*$	0.44	-1.05	$r_{A3b} = k_{A3b}\theta_{HOCO}\theta_H - k_{-A3b}\theta_{CO}\theta_{OH}$
RA4a	$HCOOH* + H* \rightarrow H_2COOH* + *$	1.39	0.33	$r_{A4a} = k_{A4a}\theta_{HCOOH}\theta_H - k_{-A4a}\theta_{H_2COOH}\theta_*$
RA4b	$CO* + H \rightarrow HCO* + *$	1.44	1.26	$r_{A4b} = k_{A4b}\theta_{CO}\theta_H - k_{-A4b}\theta_{HCO}\theta_*$
RA5a	$H_2COOH* + * \rightarrow H_2CO* + OH*$	1.00	0.92	$r_{A5a} = k_{A5a}\theta_{H_2COOH}\theta_* - k_{-A5a}\theta_{H_2CO}\theta_{OH}$
RA5b	$HCO* + H* \rightarrow H_2CO* + *$	0.85	0.21	$r_{A5b} = k_{A5b}\theta_{HCO}\theta_H - k_{-A5b}\theta_{H_2CO}\theta_*$
RA6	$OH* + H* \rightarrow H_2O* + *$	0[a]; 1.26[b]	-1.23[a]; -0.17[b]	$r_{A6} = k_{A6}\theta_{OH}\theta_H - k_{-A6}\theta_{H_2O}\theta_*$
RA7	$H_2CO* + H* \rightarrow H_3CO* + *$	1.10	0.61	$r_{A7} = k_{A7}\theta_{H_2CO}\theta_H - k_{-A7}\theta_{H_3CO}\theta_*$
RA8	$H_3CO* + H* \rightarrow CH_3OH* + *$	1.06	-0.67	$r_{A8} = k_{A8}\theta_{H_3CO}\theta_H - k_{-A8}\theta_{CH_3OH}\theta_*$
RA9	$H_2O* \rightarrow H_2O + *$	0	0.34[a]; 0.51[b]	$r_{A9} = k_{A9}\theta_{H_2O} - k_{-A9}P_{H_2O}\theta_*$
RA10	$CH_3OH* \rightarrow CH_3OH + *$	0	0.55	$r_{A10} = k_{A10}\theta_{CH_3OH} - k_{-A10}P_{CH_3OH}\theta_*$

[a] Formate pathway
[b] RWGS+CO hydrogenation pathway

Turnover frequency (TOF) is defined as the lowest reaction rate:

$$\text{TOF} = \min\{r_i\}; i = 0,1,2,..,10 \quad (5)$$

The TOF can be calculated by numerically solving a set of differential equations, which represent the rate of change in coverage for each species involved in CO_2 hydrogenation. Eqs. (6)-(16) show the examples of these differential equations for CO_2 hydrogenation in Pd_7 catalyst using formate pathway. The differential equation for other catalysts or pathways is only slightly different from these examples.

$$\frac{d\theta_H}{dt} = 2r_{A0} - (r_{A2a} + r_{A3a} + r_{A4a} + r_{A6} + r_{A7} + r_{A8}) \quad (6)$$

$$\frac{d\theta_{CO_2}}{dt} = r_{A1} - r_{A2a} \quad (7)$$

$$\frac{d\theta_{HCOO}}{dt} = r_{A2a} - r_{A3a} \quad (8)$$

$$\frac{d\theta_{HCOOH}}{dt} = r_{A3a} - r_{A4a} \quad (9)$$

$$\frac{d\theta_{H_2COOH}}{dt} = r_{A4a} - r_{A5a} \quad (10)$$

$$\frac{d\theta_{H_2CO}}{dt} = r_{A5a} - r_{A7} \quad (11)$$

$$\frac{d\theta_{OH}}{dt} = r_{A5a} - r_{A6} \quad (12)$$

$$\frac{d\theta_{H_3CO}}{dt} = r_{A7} - r_{A8} \quad (13)$$

$$\frac{d\theta_{H_2O}}{dt} = r_{A6} - r_{A9} \quad (14)$$

$$\frac{d\theta_{CH_3OH}}{dt} = r_{A8} - r_{A10} \quad (15)$$

$$\frac{d\theta_*}{dt} = (r_{A2a} + r_{A3a} + r_{A4a} + r_{A6} + r_{A7} + r_{A8} + r_{A9} + r_{A10}) - (2r_{A0} + r_{A1} + r_{A5a}) \quad (16)$$

Similar to the previous catalyst, the hydrogenation of CO_2 on the $Pd_3/TiO_2(110)$ catalyst also proceeds through two pathways: formate and RWGS+CO hydrogenation. Each pathway also has its own elementary reactions that are slightly different from those described previously. Table 2 below presents the reaction pathways, energy values, and rate equations for the CO_2 hydrogenation on the $Pd_3/TiO_2(110)$ catalyst [14]. Based on the table, it is evident that the formate pathway on this catalyst follows elementary reactions: RB0 → RB1 → RB2a → RB3a → RB4a → RB6a → RB5 → RB7 → RB8 → RB9. On the other hand, the RWGS + CO pathways for this catalyst follow these reaction steps: RB0 → RB1 → RB2b → RB3b → RB4b → RB5 → RB6b → RB7 → RB8 → RB9.

Table 2. CO_2 hydrogenation step, energies, and reaction rates equation for $Pd_3/TiO_2(110)$ [14].

Reaction Number	Reaction Notation	E_{act} [eV]	ΔE [eV]	Reaction Rates
RB0	$H_2 + 2* \rightarrow 2H*$	0.34	-1.33	$r_{B0} = k_{B0}P_{H_2}\theta_*^2 - k_{-B0}\theta_H^2$
RB1	$CO_2 + * \rightarrow CO_2*$	0	-1.49	$r_{B1} = k_{B1}P_{CO_2}\theta_* - k_{-B1}\theta_{CO_2}$
RB2a	$CO_2* + H* \rightarrow HCOO* + *$	1.63	0.66	$r_{B2a} = k_{B2a}\theta_{CO_2}\theta_H - k_{-B2a}\theta_{HCOO}\theta_*$
RB2b	$CO_2* + H* \rightarrow COOH* + *$	1.11	0.60	$r_{B2b} = k_{B2b}\theta_{CO_2}\theta_H - k_{-B2b}\theta_{COOH}\theta_*$
RB3a	$HCOO* + H* \rightarrow H_2COO* + *$	2.43	0.75	$r_{B3a} = k_{B3a}\theta_{HCOO}\theta_H - k_{-B3a}\theta_{H_2COO}\theta_*$
RB3b	$COOH* + H* \rightarrow CO* + OH*$	0.21	-1.20	$r_{B3b} = k_{B3b}\theta_{COOH}\theta_H - k_{-B3b}\theta_{CO}\theta_{OH}$
RB4a	$H_2COO* + H* \rightarrow H_2CO* + OH*$	1.88	0.23	$r_{B4a} = k_{B4a}\theta_{H_2COO}\theta_H - k_{-B4a}\theta_{H_2CO}\theta_{OH}$
RB4b	$CO* + H \rightarrow HCO* + *$	1.50	1.07	$r_{B4b} = k_{B4b}\theta_{CO}\theta_H - k_{-B4b}\theta_{HCO}\theta_*$
RB5	$OH* + H* \rightarrow H_2O* + *$	0.74	-0.04	$r_{B5} = k_{B5}\theta_{OH}\theta_H - k_{-B5}\theta_{H_2O}\theta_*$
RB6a	$H_2CO* + * \rightarrow H_3CO* + *$	1.43	1.34	$r_{B6a} = k_{B6a}\theta_{H_2CO}\theta_H - k_{-B6a}\theta_{H_3CO}\theta_*$
RB6b	$HCO* + H* \rightarrow H_2CO* + *$	0.95	0.43	$r_{B6b} = k_{B6b}\theta_{HCO}\theta_H - k_{-B6b}\theta_{H_2CO}\theta_*$
RB7	$H_3CO* + H* \rightarrow CH_3OH* + *$	0.85	0.34	$r_{B7} = k_{B7}\theta_{H_3CO}\theta_H - k_{-B7}\theta_{CH_3OH}\theta_*$
RB8	$H_2O* \rightarrow H_2O + *$	0	1.43	$r_{B8} = k_{B8}\theta_{H_2O} - k_{-B8}P_{H_2O}\theta_*$
RB9	$CH_3OH* \rightarrow CH_3OH + *$	0	1.51	$r_{B10} = k_{B10}\theta_{CH_3OH} - k_{-B10}P_{CH_3OH}\theta_*$

Hydrogenation of CO_2 in $Pd_4/In_2O_3(110)$ also goes through the same pathways which are formate and RWGS+CO. Based on the data presented in Table 3, the formate pathways in this catalyst will follow these elementary steps: RC0 → RC1 → RC2a → RC3a → RC4a → RC5a → RC6a → RC8a → RC7 → RC10 → RC11. While RWGS+CO hydrogenation pathways in $Pd_4/In_2O_3(110)$ catalyst consists of these steps: RC0 → RC1 → RC2b → RC3b → RC4b → RC5b → RC6b → RC8b → RC9 → RC10 → RC11.

Table 3. CO_2 hydrogenation step, energies, and reaction rates equation for $Pd_4/In_2O_3(110)$ [16].

Reaction Number	Reaction Notation	E_{act} [eV]	ΔE [eV]	Reaction Rates
RC0	$H_2 + 2* \rightarrow 2H*$	0	-1.08	$r_{C0} = k_{C0}P_{H_2}\theta_*^2 - k_{-C0}\theta_H^2$
RC1	$CO_2 + * \rightarrow CO_2*$	0	-0.37	$r_{C1} = k_{C1}P_{CO_2}\theta_* - k_{-C1}\theta_{CO_2}$
RC2a	$CO_2* + H* \rightarrow$ mono-HCOO* + *	1.17	0.81	$r_{C2a} = k_{C2a}\theta_{CO_2}\theta_H - k_{-C2a}\theta_{monoHCOO}\theta_*$
RC2b	$CO_2* + H* \rightarrow$ trans-COOH* + *	1.01	0.21	$r_{C2b} = k_{C2b}\theta_{CO_2}\theta_H - k_{-C2b}\theta_{transCOOH}\theta_*$
RC3a	mono-HCOO* → bi-HCOO*	0	-0.68	$r_{C3a} = k_{C3a}\theta_{monoHCOO} - k_{-C3a}\theta_{biHCOO}$
RC3b	trans-COOH* → cis-COOH*	0.39	0.01	$r_{C3b} = k_{C3b}\theta_{transCOOH} - k_{-C3b}\theta_{cisCOOH}$
RC4a	bi-HCOO* + H* → H_2COO* + *	1.09	0.75	$r_{C4a} = k_{C4a}\theta_{biHCOO}\theta_H - k_{-C4a}\theta_{H_2COO}\theta_*$
RC4b	cis-COOH* + H* → CO* + H_2O*	1.90	0.26	$r_{C4b} = k_{C4b}\theta_{cisCOOH}\theta_H - k_{-C4b}\theta_{CO}\theta_{H_2O}$
RC5a	H_2COO* + H* → H_2CO* + OH*	0.89	-1.15	$r_{C5a} = k_{C5a}\theta_{H_2COO}\theta_* - k_{-C5a}\theta_{H_2CO}\theta_{OH}$
RC5b	CO* + H* → HCO* + *	1.36	0.89	$r_{C5b} = k_{C5b}\theta_{CO}\theta_H - k_{-C5b}\theta_{HCO}\theta_*$
RC6a	H_2CO* + H* → H_2COH* + *	0.84	0.76	$r_{C6a} = k_{C6a}\theta_{H_2CO}\theta_H - k_{-C6a}\theta_{H_2COH}\theta_*$
RC6b	HCO* + H* → H_2CO* + *	0.82	0.21	$r_{C6b} = k_{C6b}\theta_{HCO}\theta_H - k_{-C6b}\theta_{H_2CO}\theta_*$
RC7	OH* + H* → H_2O*	0.98	-0.65	$r_{C7} = k_{C7}\theta_{OH}\theta_H - k_{-C7}\theta_{H_2O}$
RC8a	H_2COH* + H* → CH_3OH* + *	1.11	0.20	$r_{C8a} = k_{C8a}\theta_{H_2COH}\theta_H - k_{-C8a}\theta_{CH_3OH}\theta_*$
RC8b	H_2CO* + H* → H_3CO* + *	0.41	0.03	$r_{C8b} = k_{C8b}\theta_{H_2CO}\theta_H - k_{-C8b}\theta_{H_3CO}\theta_*$
RC9	H_3CO* + H* → CH_3OH* + *	1.33	0.24	$r_{C9} = k_{C9}\theta_{H_3CO}\theta_H - k_{-C9}\theta_{CH_3OH}\theta_*$
RC10	H_2O* → H_2O + *	0	0.58	$r_{C10} = k_{C10}\theta_{H_2O} - k_{-C10}P_{H_2O}\theta_*$
RC11	CH_3OH* → CH_3OH + *	0	0.78	$r_{C11} = k_{C11}\theta_{CH_3OH} - k_{-C11}P_{CH_3OH}\theta_*$

The activation barriers and reaction energies summarized in Tables 1, 2, and 3 are used as inputs for microkinetic modeling to calculate the TOF for CO_2 hydrogenation to methanol on each catalyst.

Results and Discussion

The TOF as a function of temperature for CO_2 hydrogenation to methanol on Pd_7, $Pd_3/TiO_2(110)$, and $Pd_4/In_2O_3(110)$ has been calculated for both the formate and the RWGS+CO hydrogenation pathways. The results are shown in Fig. 2. The TOF was calculated under typical conditions used for CO_2 hydrogenation on standard Cu-based catalyst, that is at p = 75 bar with a CO_2:H_2 pressure ratio of 1:3. These results show that the TOF for the formate pathway on $Pd_4/In_2O_3(110)$ and Pd_7 is higher than that for the RWGS+CO hydrogenation pathway. This means that for both catalysts the CO_2 hydrogenation tends to be more selective towards the formate pathway. This finding is consistent with the result from previous studies by Ye et al. [16] and Saputro et al. [4]. However, at temperatures below 700 K, the TOF for the RWGS+CO hydrogenation pathway on the $Pd_3/TiO_2(110)$ is higher than the TOF for the formate pathway. This indicates that $Pd_3/TiO_2(110)$ is more selective towards the RWGS+CO hydrogenation pathway in this temperature range. It also means that the addition of certain supports can change the dominant pathway to the RWGS+CO hydrogenation rather than the formate pathway. This agrees with the results of the thermodynamic study by Ou et al. which showed that RWGS+CO hydrogenation is more dominant than the formate pathway on the $Pd_3/TiO_2(110)$ catalyst [14]. Comparing the TOF of the best pathway between the three catalysts (formate pathway on Pd_7 and $Pd_4/In_2O_3(110)$, and RWGS+CO hydrogenation on $Pd_3/TiO_2(110)$), $Pd_4/In_2O_3(110)$ has the highest TOF over the whole temperature range, while $Pd_3/TiO_2(110)$ has the lowest TOF. This

shows that the presence of the right metal oxide support can increase the reaction rate of CO_2 hydrogenation, thus improving the catalytic activity of Pd clusters.

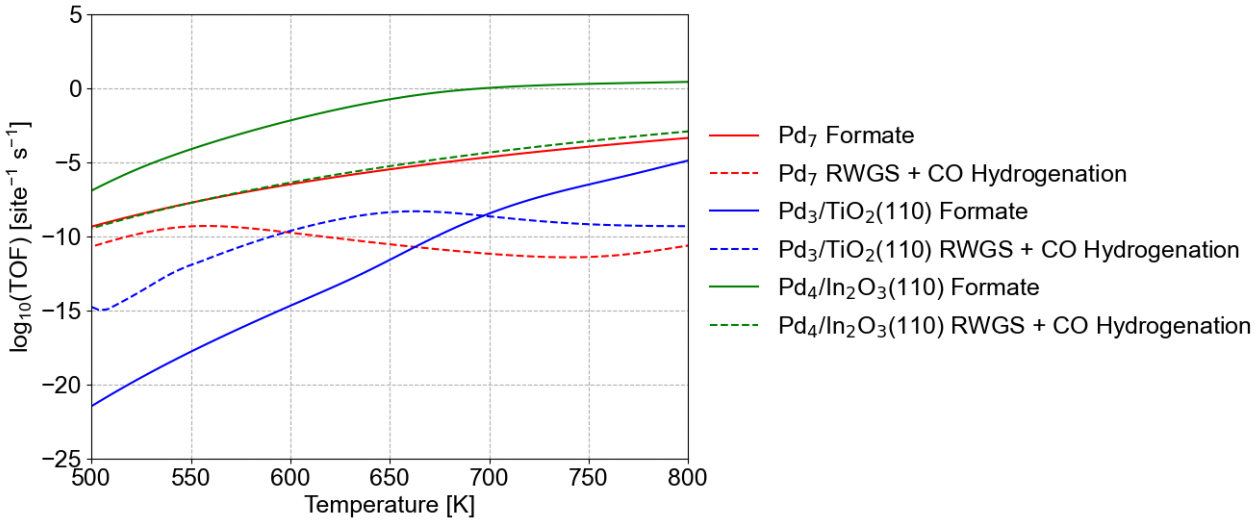

Fig. 1. TOF profiles as a function of temperature for CO_2 hydrogenation to methanol via formate and RWGS+CO hydrogenation pathways over Pd_7, $Pd_3/TiO_2(110)$, and $Pd_4/In_2O_3(110)$. TOF was calculated at p = 75 bar with CO_2:H_2 pressure ratio of 1:3.

The surface coverage profiles versus temperature of each species involved in the CO_2 hydrogenation reaction via the formate pathway and the RWGS+CO hydrogenation pathway is shown in Fig 3. We can see that the dominating coverage for each pathway is different. For Pd_7 in the formate pathway (Fig. 3a) and $Pd_4/In_2O_3(110)$ in both pathways (Fig. 3c and f), there is a high H* coverage in the low temperature region which indicates that H* has not been consumed. The H* coverage decreases as the temperature increases, indicating that more H* is consumed. Meanwhile, from the surface coverage profile for $Pd_3/TiO_2(110)$ (see Fig. 3b and e), there is a high CO_2* coverage at temperatures lower than 700 K, where the formate pathway has a higher CO_2* coverage than the RWGS+CO hydrogenation pathway. This explains why the RWGS+CO hydrogenation pathway on $Pd_3/TiO_2(110)$ catalyst exhibits higher TOF than the format pathway at temperatures lower than 700 K. Furthermore, we can see that for the RWGS+CO hydrogenation pathway on Pd_7 (Fig. 3d) and Pd_3/TiO_2 (Fig. 3e) there is CO* poisoning. For Pd_7 catalyst, CO* poisoning has occurred even in the low temperature region so that the RWGS+CO hydrogenation pathway on Pd_7 has a lower TOF than the formate pathway. Meanwhile, for Pd_3/TiO_2, CO* poisoning occurs at temperatures higher than 700 K. This causes the RWGS pathway to produce a lower TOF than the formate pathway at temperatures higher than 700 K.

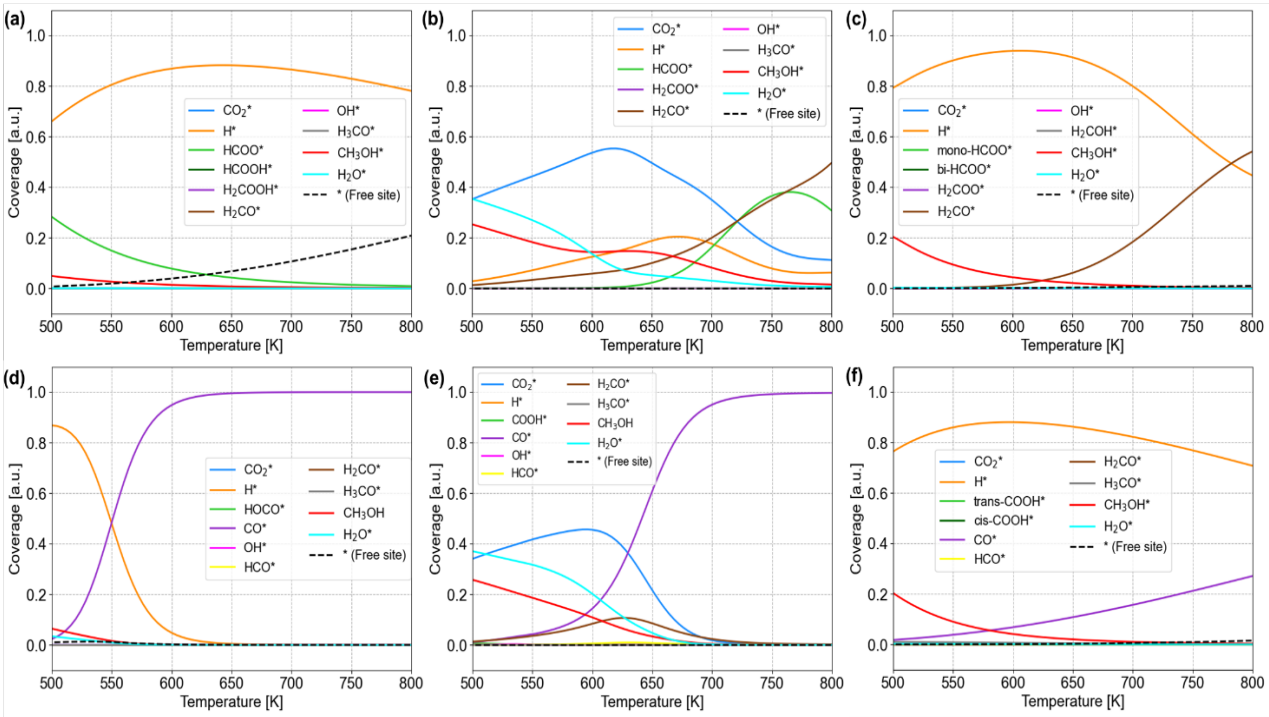

Fig. 2. Surface coverage of each species involved in CO_2 hydrogenation via the formate pathway on (a) Pd_7, (b) $Pd_3/TiO_2(110)$, (c) $Pd_4/In_2O_3(110)$, and via the RWGS+CO hydrogenation pathway on (d) Pd_7, (e) $Pd_3/TiO_2(110)$, and (f) $Pd_4/In_2O_3(110)$.

Conclusions

In this work, we study the kinetics of CO_2 hydrogenation to produce methanol on Pd_7 cluster (without support), $Pd_4/In_2O_3(110)$, and $Pd_3/TiO_2(110)$ using microkinetic model. Our results show that the presence of metal oxide support on subnanometer Pd_x cluster can improve the reaction rate of CO_2 hydrogenation, as Pd_4/In_2O_3 can produce higher TOF than Pd_7 cluster. Furthermore, the presence of a support can also alters the dominant reaction pathway. For example, Pd_3/TiO_2 can change the pathway to be more selective towards RWGS+CO hydrogenation than formate pathway. Therefore, the type of support material must be considered in designing a catalyst for CO_2 hydrogenation with the desired catalytic activity.

Acknowledgments

We acknowledge the research fund granted by Institut Teknologi Bandung, under grant scheme “Riset Unggulan ITB 2023”.

References

[1] P. Schwiderowski, H. Ruland, M. Muhler, Current developments in CO2 hydrogenation towards methanol: A review related to industrial application, Curr Opin Green Sustain Chem 38 (2022) 100688.

[2] M. Takht Ravanchi, S. Sahebdelfar, Catalytic conversions of CO2 to help mitigate climate change: Recent process developments, Process Safety and Environmental Protection 145 (2021) 172–194.

[3] C. Mebrahtu, F. Krebs, S. Abate, S. Perathoner, G. Centi, R. Palkovits, Chapter 5 - CO2 Methanation: Principles and Challenges, in: S. Albonetti, S. Perathoner, E.A. Quadrelli (Eds.), Stud Surf Sci Catal, Elsevier, 2019: pp. 85–103.

[4] A.G. Saputro, A.L. Maulana, F. Fathurrahman, G. Shukri, M.H. Mahyuddin, M.K. Agusta, T.D.K. Wungu, H.K. Dipojono, Density functional and microkinetic study of CO2 hydrogenation to methanol on subnanometer Pd cluster doped by transition metal (M= Cu, Ni, Pt, Rh), Int J Hydrogen Energy 46 (2021) 14418–14428.

[5] A.G. Saputro, R.I.D. Putra, A.L. Maulana, M.U. Karami, M.R. Pradana, M.K. Agusta, H.K. Dipojono, H. Kasai, Theoretical study of CO2 hydrogenation to methanol on isolated small Pdx clusters, Journal of Energy Chemistry 35 (2019) 79–87.

[6] F. Brix, V. Desbuis, L. Piccolo, É. Gaudry, Tuning Adsorption Energies and Reaction Pathways by Alloying: PdZn versus Pd for CO2 Hydrogenation to Methanol, J Phys Chem Lett 11 (2020) 7672–7678.

[7] D. Guo, J. Liu, X. Zhao, X. Yang, X. Chen, Comparative computational study of CO2 hydrogenation and dissociation on metal-doped Pd clusters, Sep Purif Technol 313 (2023) 123462.

[8] N. Garg, A. Sarkar, B. Sundararaju, Recent developments on methanol as liquid organic hydrogen carrier in transfer hydrogenation reactions, Coord Chem Rev 433 (2021) 213728.

[9] H. Li, L. Wang, X. Gao, F.-S. Xiao, Cu/ZnO/Al2O3 Catalyst Modulated by Zirconia with Enhanced Performance in CO2 Hydrogenation to Methanol, Ind Eng Chem Res 61 (2022) 10446–10454.

[10] K. Stangeland, H. Li, Z. Yu, CO2 hydrogenation to methanol: the structure–activity relationships of different catalyst systems, Energy Ecol Environ 5 (2020) 272–285.

[11] J. Zhong, X. Yang, Z. Wu, B. Liang, Y. Huang, T. Zhang, State of the art and perspectives in heterogeneous catalysis of CO2 hydrogenation to methanol, Chem Soc Rev 49 (2020) 1385–1413.

[12] T.P. Araújo, S. Mitchell, J. Pérez-Ramírez, Design Principles of Catalytic Materials for CO2 Hydrogenation to Methanol, Advanced Materials (2024) 2409322.

[13] X. Jiang, X. Nie, X. Guo, C. Song, J.G. Chen, Recent Advances in Carbon Dioxide Hydrogenation to Methanol via Heterogeneous Catalysis, Chem Rev 120 (2020) 7984–8034.

[14] Z. Ou, J. Ran, J. Niu, C. Qin, W. He, L. Yang, A density functional theory study of CO2 hydrogenation to methanol over Pd/TiO2 catalyst: The role of interfacial site, Int J Hydrogen Energy 45 (2020) 6328–6340.

[15] O.A. Ojelade, S.F. Zaman, A Review on Pd Based Catalysts for CO2 Hydrogenation to Methanol: In-Depth Activity and DRIFTS Mechanistic Study, Catalysis Surveys from Asia 24 (2020) 11–37.

[16] J. Ye, C. Liu, D. Mei, Q. Ge, Methanol synthesis from CO2 hydrogenation over a Pd4/In2O3 model catalyst: A combined DFT and kinetic study, J Catal 317 (2014) 44–53.

[17] H. Eyring, The Activated Complex in Chemical Reactions, J Chem Phys 3 (1935) 107–115.